Assessment of Pluvial Flood Resilience in Urban Residential Areas Based on Residents' Travel Disruption Characteristics and Planning Implications: A Case Study of Shenzhen

Authors

CHENG Yulin, GAN Xinyue, YANG Xiaochun, GUO Renzhong

Abstract

Residential neighborhoods are fundamental units for analyzing urban safety resilience and its spatial differentiation. Existing studies rely largely on static data for macro-scale assessment and therefore struggle to capture the dynamic evolution of urban resilience at fine spatial scales. This study uses residents' spatiotemporal mobility disruption during disasters as the core indicator of resilience and develops a data-driven framework for assessing pluvial flood resilience at the neighborhood scale. Based on mobile phone signaling data, the framework is applied to 1,087 residential neighborhoods in Shenzhen during the concentrated rainfall period of the 2023 "9.7" extreme rainstorm. The results show that commodity-housing neighborhoods have significantly higher resilience than urban villages, while neighborhoods built in different periods display clear heterogeneity in both disaster-time and post-disaster resilience. Correlation analysis confirms that road waterlogging is an important driver of residents' travel disruption and validates the effectiveness of the framework in identifying spatial differences in neighborhood resilience. Demographic validation further reveals that applying mobile phone signaling data to micro-scale resilience assessment may underestimate the real risks faced by aging neighborhoods. The proposed framework provides quantitative support for dynamic disaster monitoring and early warning, urban renewal diagnostics, and sustainable planning.

Keywords

residential-neighborhood pluvial flood resilience; mobile phone signaling data; travel disruption; spatial differentiation; assessment framework

Introduction

Against the background of increasingly extreme global climate conditions, urban climate resilience has become a central issue in both international scholarship and governance practice. As the basic unit of urban governance, the residential neighborhood is not only the spatial carrier of everyday life, but also the front line of disaster emergency management. International metropolises such as London and New York have incorporated the strengthening of neighborhood capacity to withstand natural hazards into major climate-adaptation strategies [1]. In recent years, however, China's superlarge and megacities have experienced frequent extreme rainstorms. Climate systems may maintain active residual circulation through a "train effect," allowing intermittent rainfall to generate continuing secondary impacts [2]. Such events seriously constrain the normal operation of urban functions, including residents' production and daily life, and delay post-disaster recovery.

Existing studies often assess macro-scale urban resilience through static indicators, making it difficult to dynamically identify differences in resilience across the full disaster cycle at the neighborhood scale. This study therefore introduces residents' spatiotemporal travel-disruption characteristics and constructs a data-driven assessment framework for pluvial flood resilience in urban residential neighborhoods. The framework is used to analyze Shenzhen's 2023 "9.7" extreme rainstorm. It identifies the spatiotemporal heterogeneity of resilience among different neighborhood types, validates the model using actual road-waterlogging data, and reveals potential bias in big-data applications for micro-scale resilience assessment. The method aims to provide scientific support for refined emergency response, neighborhood renewal diagnostics, and climate-adaptive planning.

1. Review of Urban Pluvial Flood Resilience Assessment Methods

Urban resilience research has experienced a paradigm shift from vulnerability to resilience [3]. Earlier studies [4-6] mostly inherited the traditional vulnerability framework based on composite indicator systems and focused on pre-disaster intrinsic attributes. Because of limits in data availability, indicator selection and weighting inevitably involved subjective bias. After Cutter et al. [7-9] developed the Social Vulnerability Index and the Baseline Resilience Indicators for Communities, research attention shifted from static assessment toward dynamic system response. Many scholars have since used multi-source spatiotemporal data to capture the process characteristics of urban resilience.

Urban pluvial flood resilience refers to the comprehensive ability of an urban system to resist, absorb, adapt to, and recover from the impacts of rainstorm and flood disasters [10-11]. Consistent with the broader concept of resilience, its core meaning usually includes three dimensions: effectively reducing performance decline during a disaster, recovering rapidly from disturbance, and achieving a relatively high recovery level [12-15]. Its spatial scale covers individuals or buildings, communities, cities, and regions [16-18]. Whether through scenario analysis based on simulation software [19], system-dynamics methods using social network analysis [20], empirical analysis based on big data [21-24], or resilience curves [25], resilience quantification has become a widely used theoretical tool.

Research based on resilience curves can systematically capture the temporal trajectory of system performance before and after disasters. By extracting key points such as impact points, recovery points, and stabilization points, it quantifies total disturbance area, peak loss rate, recovery rate, and curve shape [26-29]. This approach has become a core paradigm in resilience studies and has been applied to describe the dynamic response of critical urban functions such as transport networks, drainage, power supply, medical facilities, and economic output [30]. Big data provide high-resolution support for analyzing the spatiotemporal behavior of urban populations and are increasingly applied to behavioral modeling during disasters. Existing studies have extended resilience-curve frameworks using social media, GPS trajectories, and mobile phone signaling data. Some use daily units to identify long-term macro-disturbance and bimodal recovery patterns [22]; others use hourly units to capture the short-term impact of extreme rainstorms and find that system recovery may lag behind the end of the event [23], or identify delayed recovery effects in mobility network flows [24]. These studies reveal travel-disruption characteristics caused by extreme weather, but their treatment of multi-stage disaster impacts remains insufficient.

Existing research often combines disaster-time impact and post-disaster recovery into a single disturbance measure, which makes it difficult to distinguish the drivers and cumulative effects of the two stages and therefore blurs the understanding of disaster mechanisms. In particular, dynamic resilience assessment at the neighborhood scale still lacks suitable methods. Few studies can effectively quantify the impacts of rainstorm disasters on residents' travel behavior across different stages [31]. To address this gap, this study constructs short-cycle neighborhood travel fluctuation curves before and after a disaster at an hourly scale [32]. It uses the timing of waterlogging clearance to separate stages. The conventional resistance and recovery stages are treated as the disaster-time stage to quantify direct impact, while a lagged-disturbance stage is added as the post-disaster stage to capture secondary effects. This approach matches the multi-stage climatic characteristics of extreme rainstorms, enables dynamic assessment of resilience among different types of urban neighborhoods, and supports the translation of fine-grained diagnosis into emergency governance and planning implications [33].

2. Empirical Study Area and Research Methods

2.1 Study Area, Data Sources, and Processing

According to the Shenzhen Meteorological Observatory, from 17:00 on September 7 to 6:00 on September 8, 2023, Shenzhen experienced an extreme rainstorm that exceeded historical records. The strong convective system showed a pronounced "train effect," and intermittent rainfall continued to affect the post-disaster recovery process. This study selects 14 subdistricts with concentrated rainfall as the study area, including the whole of Luohu District, the Yuangang, Huaqiangbei, and Nanyuan subdistricts in Futian District, and Buji Subdistrict in Longgang District (Figure 1).

Using residential-neighborhood area-of-interest data from Baidu Maps as the base, combined with OpenStreetMap data, Shenzhen building vector data from 2018, and commodity-housing coordinate points from the Anjuke platform, the study identifies and screens 1,087 residential neighborhood units in the study area, including 103 urban villages and 984 commodity-housing neighborhoods (Figure 1(b)).

Residents' travel characteristics are derived from mobile phone signaling data provided by the China Unicom Smart Footprint DAAS platform. The dataset contains approximately one million anonymized device movement traces in the study area before and after the rainstorm, from September 2 to September 24, 2023.

In addition, road-waterlogging information during the 2023 "9.7" rainstorm released by the Shenzhen Water Affairs Bureau and the Emergency Management Bureau, together with street-level demographic structure data from the 2020 Seventh National Population Census, is used to validate the reliability of the assessment method.

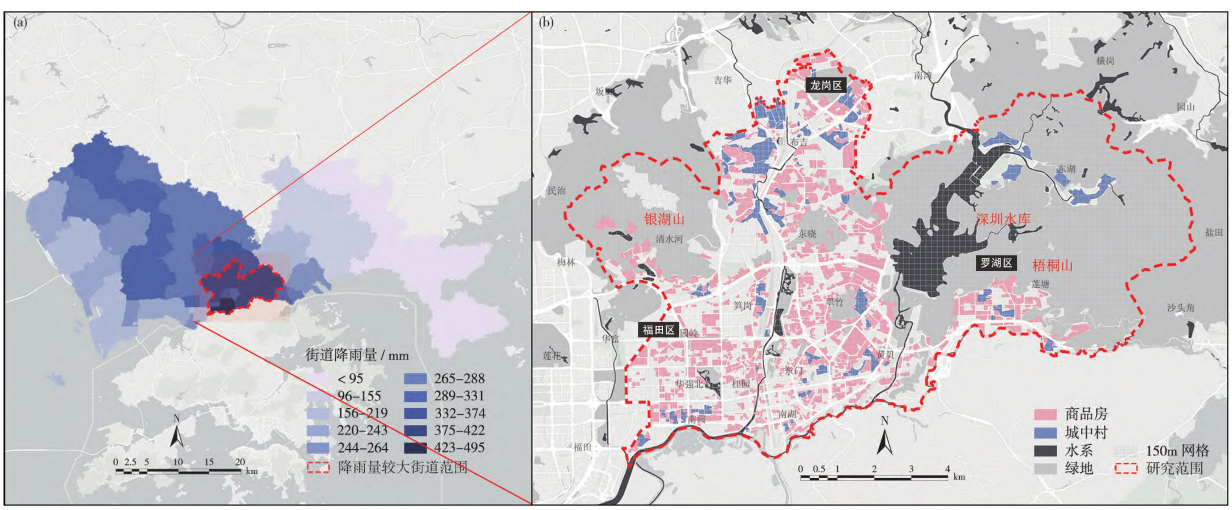

（a）深圳“9·7”极端暴雨24 h降雨量空间分布示意图　　（b）研究范围内住区空间单元分布图

Figure 1. Study Area

The figure includes a 24-hour spatial distribution map of rainfall during Shenzhen's "9.7" extreme rainstorm and a map of residential-neighborhood spatial units within the study area.

2.2 Research Methods

This study quantifies the degree to which residential neighborhoods are affected by extreme rainstorms and their ability to recover by calculating changes in residents' travel volume during the disaster compared with non-disaster periods. It then combines road-waterlogging data, walking catchments, external road connectivity, and street-level demographic structure for multi-dimensional validation. The assessment process contains three key steps (Figure 2).

2.2.1 Construction of the Travel Database

The study uses structured query language (SQL) on the DAAS platform to collect anonymized spatiotemporal information records, ensuring lawful data use and strict protection of user privacy. Residential-neighborhood boundary data are imported into the platform, and SQL is used to calculate each neighborhood's hourly total travel volume, forming a neighborhood travel database covering the pre-disaster, disaster-time, and post-disaster periods.

The study selects travel-volume changes from September 6 to September 15, 2023, a continuous 10-day period, as the basis for travel fluctuation curves. This period covers the rainstorm and one subsequent working week, allowing the study to capture persistent post-disaster mobility trends. To avoid special holidays, September 5, the sunny day before disaster warning, and the hourly average from September 18 to September 22 after the event stabilized are selected as the non-disaster weekday baseline. September 2 and September 3, and September 23 and September 24, are used to calculate non-disaster Saturday and Sunday baselines. Together these form three hourly travel baselines for each neighborhood: weekday, Saturday, and Sunday.

A moving average is used to generate travel fluctuation curves. The window is set at 7 hours to smooth noise while retaining disaster trends. Preliminary analysis shows that more than 50% of neighborhoods exhibit a staged travel-disruption pattern of "disaster-time impact plus lagged disturbance."

2.2.2 Assessment and Classification of Neighborhood Pluvial Flood Resilience

Following the core logic of resilience curves, the study measures how the system performs in response to a disaster over continuous time. It analyzes changes in residents' hourly travel volume before and after the rainstorm, and inversely represents neighborhood pluvial flood resilience through the degree of disruption to residents' travel behavior. The method is adaptively optimized according to the climatic characteristics of the "9.7" rainstorm.

First, a lagged-disturbance stage is introduced to capture the secondary impacts of rainstorm disasters on residents' travel. The effect of rainstorms on mobility is often multi-stage: an initial direct rainfall impact is followed by lagged effects caused by intermittent rainfall, and travel may remain disrupted for several days after the main rainfall ends. Therefore, unlike earlier resilience studies that focus mainly on a single shock, this study incorporates lagged disturbance as a post-disaster stage in resilience indicator calculation, allowing a more complete depiction of neighborhood resilience across different stages of the rainstorm and its secondary impacts.

Second, the non-disaster travel fluctuation range is used to determine disaster-characteristic points. Because residents' daily travel varies naturally, the impact point and stabilization point are not zero points, but intersections with the normal fluctuation range. The study defines the difference in travel volume at hour t as Delta St, calculates the standard deviation sigma of the difference sequence, and uses sigma as the reference boundary of the non-disaster fluctuation range.

Third, the study constructs a per capita travel-disruption intensity measure that strengthens the cumulative effect of duration. According to the difference in disturbance intensity and duration, disturbance is divided into short-term high-intensity and long-term medium-intensity types. The longer the duration, the more types of travel activities are affected, and the stronger the cumulative consumption of resources and socioeconomic loss. Therefore, disturbance intensity A is time-weighted. The composite indicator highlights the cumulative cost of travel disruption across the disaster cycle [35] and is normalized into "per capita travel-disruption intensity" to enable comparison across neighborhoods (Table 1). Compared with traditional indicators, this measure is more sensitive to resilience differences among small spatial units.

According to the Shenzhen Meteorological Bureau's summary [Note 1], 48 hours is used as the dividing line between the disaster-time and post-disaster stages. Disaster-time disturbance is the sum of all travel disturbance before the 48-hour line, and post-disaster disturbance is calculated in the same way after it. If a disturbance crosses the 48-hour line, it is assigned according to the larger area before or after the line. Finally, K-means clustering is used to classify disaster-time and post-disaster resilience separately, while the Elbow Method and silhouette coefficient determine the optimal number of clusters.

Table 1. Indicator Algorithms

Indicator	Formula	Meaning
Non-disaster fluctuation range	sigma = sqrt((1/N) * sum_t(Delta St - mean(Delta S))^2), N = 24 h	Sigma is calculated from the difference in travel volume between two comparable normal travel days within 24 hours. It is used as the reference boundary for non-disaster travel fluctuation.
Per capita travel-disruption intensity	V1 = A1 / (Ni *T1); A1 = integral from t0 to t2 of [max(0, Qmax - Qt - sigma)] dt* (t2 - t0)	V1 is the per capita travel-disruption intensity of the initial fluctuation in neighborhood i; Ni is the total population of the neighborhood; A1 is the initial disturbance intensity and reflects the cumulative effect of travel decline from impact point to stabilization point; T1 is the duration of disturbance; Qmax is the travel baseline and Qt is actual resident travel volume.

2.2.3 Validation of the Assessment Method

To validate the applicability and reliability of the assessment method in real scenarios, the study introduces multi-dimensional external variables for empirical testing.

First, it analyzes road-waterlogging proximity and external road connectivity. Residents often cancel trips when travel routes are blocked by waterlogged roads. Neighborhoods close to waterlogged roads and with low route choice, operationalized as weak external road connectivity, are expected to experience greater functional loss and travel constraints under rainstorm waterlogging. To test this hypothesis, the study constructs walking-accessibility buffer zones to waterlogged roads using thresholds of more than 15 minutes, 10-15 minutes, 5-10 minutes, and less than 5 minutes. A chi-square test is used to examine the significance of the association between resilience grade and proximity to waterlogged roads. Based on space syntax, betweenness centrality, which represents the structural importance of the road network, and angular mean depth, which represents path-organization efficiency, are used to characterize external road connectivity. Neighborhoods are divided into low- and high-connectivity groups, and stratified chi-square tests are conducted to analyze the interaction between road-waterlogging proximity and external road connectivity.

It should be noted that neighborhood elevation is not included as a main validation variable. Although elevation is a traditional physical factor in waterlogging distribution, its relationship with water depth and travel restriction is affected by drainage systems, pipe-network capacity, microtopography, soil permeability, and emergency arrangements. The relationship is therefore not simply linear. Moreover, neighborhood elevation mainly reflects the risk of the neighborhood itself being flooded, while it is not a direct explanatory factor for residents' travel being affected by flood conditions.

Second, demographic structure at the street level is used for validation. To test whether mobile phone signaling data contain representation bias at the neighborhood scale for vulnerable groups such as older adults, children, and some low-income floating populations, and to explore the social interpretability of the proposed method, the study introduces street-level demographic structure data from Shenzhen's Seventh National Population Census. These include the share of residents aged 65 and above, the share of children aged 0-14, and the average years of schooling among residents aged 15 and above. Spearman rank correlation analysis is used to test the strength and significance of the relationship between average street-level resilience and demographic structure.

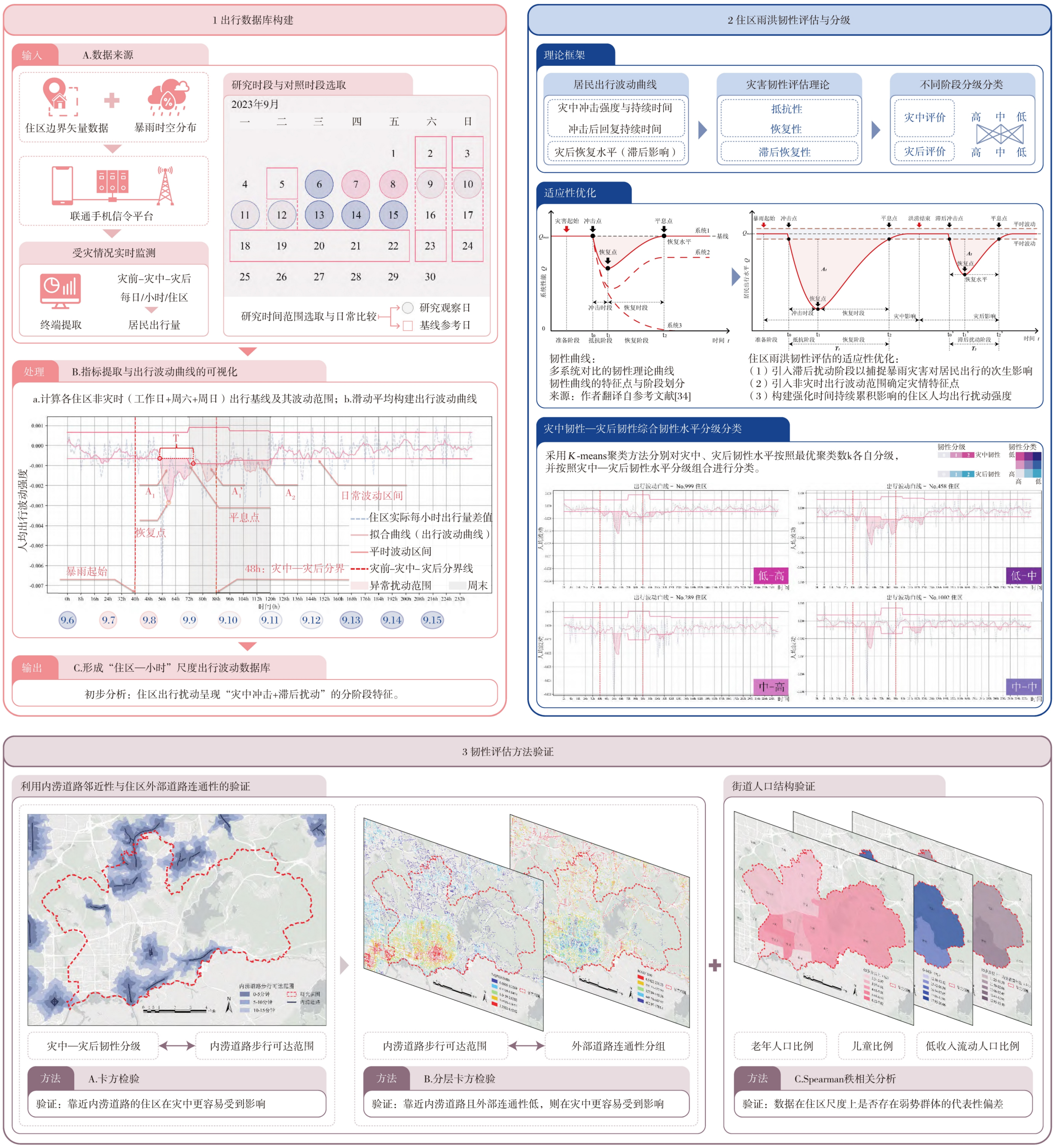

Figure 2. Research Methods

The method integrates three modules: travel database construction, neighborhood pluvial flood resilience assessment and classification, and validation of the assessment method. It compares disaster-time and non-disaster travel curves, distinguishes disaster-time and post-disaster stages, applies K-means resilience classification, and validates results through waterlogged-road buffers, external road connectivity, and street-level demographic structure.

3. Research Results

3.1 Disaster-Time and Post-Disaster Neighborhood Resilience Levels

Clustering results for per capita travel-disruption intensity during and after the disaster show that the sum-of-squared-error curves both display an elbow at k = 3, while silhouette coefficients are also relatively high. Therefore, disaster-time and post-disaster resilience levels are each divided into three grades, labeled 0, 1, and 2 to represent high, medium, and low resilience, and neighborhoods are further classified according to combined disaster-time and post-disaster grades.

The resilience maps (Figure 3) show that low-resilience neighborhoods present contiguous spatial patterns. Disaster-time low-resilience neighborhoods are concentrated mainly in Liantang Subdistrict of Luohu District and in the border areas among Dongmen, Huangbei, and Nanhu subdistricts. These areas are relatively low-lying, and drainage systems may not be able to withstand short-duration intense rainfall, resulting in severe waterlogging and direct impacts on residents' travel. Newly emerging post-disaster low-resilience neighborhoods are concentrated mainly in Guiyuan Subdistrict of Luohu District and Nanyuan Subdistrict of Futian District. These areas are close to commercial clusters and may be affected by traffic congestion and dense socioeconomic activity, allowing travel disruption to continue after the rainstorm. Neighborhoods with low resilience in both disaster-time and post-disaster stages are concentrated in Buji Subdistrict of Longgang District, where many old communities and urban villages are located. Aging infrastructure and inadequate drainage systems make these areas prone to waterlogging and intensify persistent travel disruption during and after the event. In addition, areas such as Sungang and Qingshuihe in Luohu District show small contiguous clusters, while a small number of low-resilience neighborhoods appear as isolated cases. These patterns reflect the potential influence of infrastructure level, governance efficiency, and terrain differences on resilience distribution.

Cross-area comparison further shows that low-resilience neighborhoods in the study area are concentrated mainly in Luohu and Longgang, while Futian, with stronger economic conditions, has significantly fewer low-resilience neighborhoods. This result reflects the deep influence of urban spatial form, built-environment infrastructure, and economic resource allocation on neighborhood disaster resistance. A comparison between commodity housing and urban villages shows that low-resilience neighborhoods are mainly urban villages. Some urban villages have much lower resilience than adjacent commodity-housing neighborhoods, indicating serious infrastructure deficits in parts of the urban-village built environment and highlighting their resilience disadvantage under the same geographical conditions.

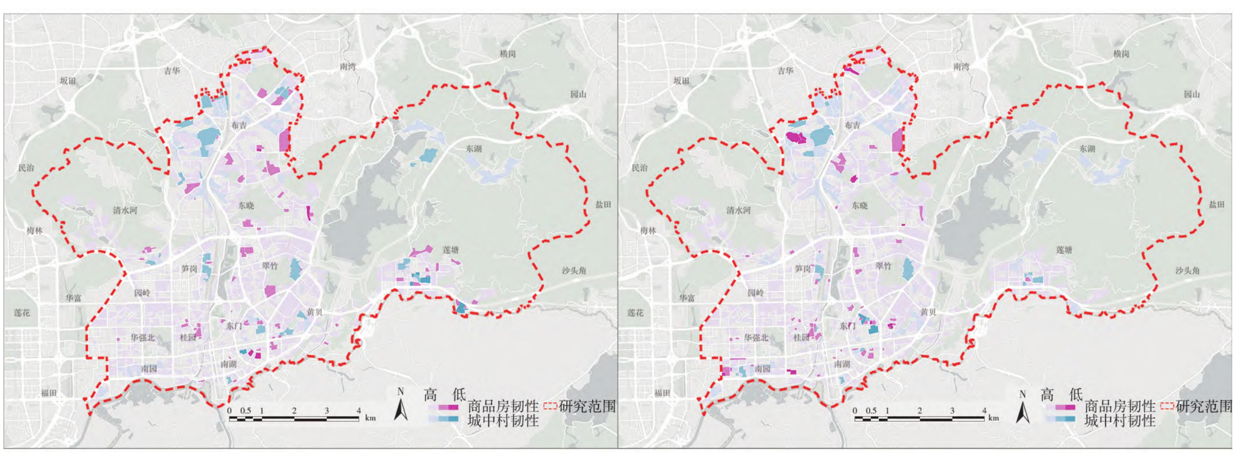

Figure 3. Maps of Residential Neighborhood Resilience

The figure presents neighborhood resilience maps during the disaster and after the disaster, identifying contiguous low-resilience areas and their differences across Luohu, Futian, and Longgang.

3.2 Differences in Disaster-Time and Post-Disaster Resilience Across Neighborhood Types

Based on the resilience assessment results, this study generates boxplots and scatter distributions to analyze resilience changes among different types of neighborhoods during and after the disaster, revealing their differentiated resilience characteristics (Figure 4).

Urban villages show lower overall disaster-time and post-disaster resilience. The boxplot indicates that the upper whisker of disaster-time disturbance is significantly extended, and several extremely high-disruption samples widen the distribution range (Figure 4(a)). This may be attributed to insufficient infrastructure and limited social resources, which amplify disaster impacts. Although post-disaster disturbance declines, it remains relatively high and approaches the disaster-time disturbance level of commodity-housing neighborhoods, indicating stronger lagged effects during recovery in urban villages. By contrast, commodity-housing neighborhoods have a lower median disaster-time disturbance, although the scatter plot still shows some low-resilience samples. Their post-disaster disturbance decreases significantly, possibly because better infrastructure and sufficient social resource support enable more efficient recovery.

The boxplot by construction period (Figure 4(b)) shows that commodity-housing neighborhoods built before 2000 and those built between 2000 and 2010 have similar overall resilience. However, the scatter plot reveals more low-resilience samples among pre-2000 neighborhoods, likely because of aging infrastructure and insufficient social support. Commodity-housing neighborhoods built between 2000 and 2010 recover faster after the disaster, benefiting from improved planning standards and a gradually upgraded built environment. Neighborhoods built after 2010 show the highest median disaster-time travel disruption and a larger interquartile range, but they contain the fewest low-resilience scattered samples and recover fastest after the disaster. This pattern is consistent with better infrastructure and resource allocation.

Although conventional assumptions suggest a positive correlation between construction period, neighborhood quality, and resilience, this study finds that disaster-time resilience differences reveal nonlinear heterogeneity in resistance capacity and population response mechanisms under rainstorm impact. Overall, neighborhood resilience assessment should move beyond single built-environment indicators and consider the dynamic changes in disaster-time resistance and post-disaster recovery. The low resilience of urban villages highlights the importance of socioeconomic attributes and emergency resource allocation, while differences across commodity-housing construction periods reveal the influence of infrastructure evolution.

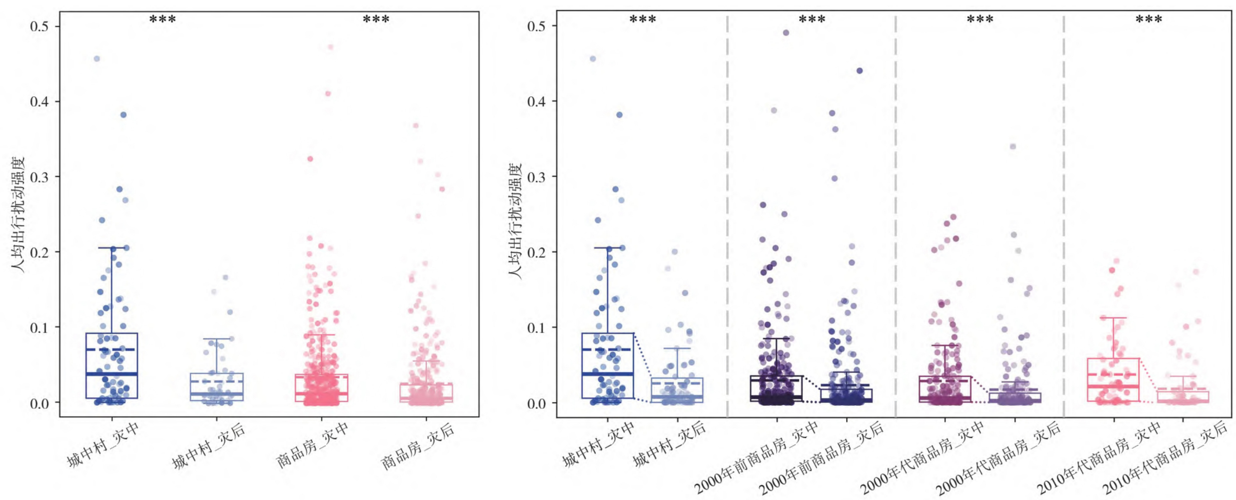

（a）城中村与商品房韧性对比

（b）城中村与各个年代的商品房韧性对比

Figure 4. Boxplot and Scatter Distribution of Resilience Levels for Residential Areas

The figure compares resilience between urban villages and commodity-housing neighborhoods, and further compares urban villages with commodity-housing neighborhoods built in different periods.

3.3 Validation of Neighborhood Resilience Assessment Results

The chi-square test results (Figure 5) show that disaster-time resilience is significantly associated with walking distance to waterlogged roads (chi-square = 14.5216, P = 0.0243 < 0.05). Neighborhoods closer to waterlogged roads have a significantly higher probability of low resilience during the disaster. The association between post-disaster resilience and walking distance to waterlogged roads is not significant (chi-square = 12.0748, P = 0.0603 > 0.05), showing only a marginal trend. This supports the validity of the assessment method: disaster-time resilience is directly affected by road waterlogging, whereas post-disaster resilience is influenced by other factors.

The stratified chi-square tests divide neighborhoods into low- and high-connectivity groups by the median external connectivity. Results show that in the low-connectivity group, disaster-time resilience is significantly associated with walking distance to waterlogged roads (chi-square = 15.8262, P = 0.01472 < 0.05). In the high-connectivity group, this association is not significant (chi-square = 9.0223, P = 0.1723 > 0.05), indicating that the impact of waterlogging is weakened when external connectivity is high. For post-disaster resilience, neither the low-connectivity group (chi-square = 10.8070, P = 0.0945 > 0.05) nor the high-connectivity group (chi-square = 7.3557, P = 0.2892 > 0.05) shows a significant association with walking distance to waterlogged roads. These findings reveal that external road connectivity is an important moderator of the effect of waterlogged roads on disaster-time resilience. Neighborhoods with low connectivity are more likely to experience severe travel constraints when nearby roads are waterlogged, while highly connected neighborhoods can mitigate impacts through alternative routes and drainage pathways. The results jointly demonstrate that the proposed method can effectively capture the differentiated impact of waterlogged roads on disaster-time resilience in surrounding neighborhoods.

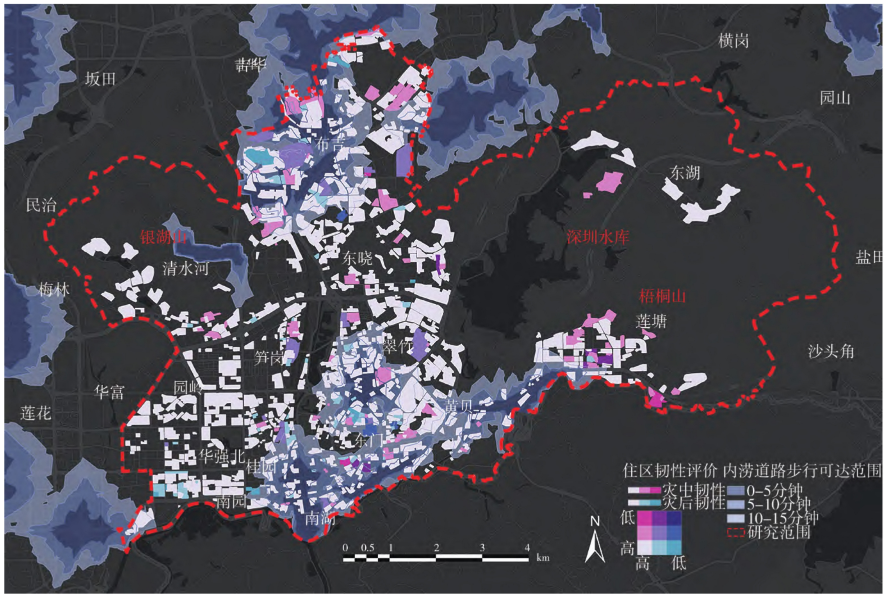

Figure 5. Validation Using Layered Buffer Zones Around Waterlogged Roads

The figure validates the association between neighborhood resilience, walking distance to waterlogged roads, and external road connectivity during the disaster and after the disaster.

Spearman rank correlation results between average street-level resilience indicators and demographic structure variables are shown in Table 2. The disaster-time disturbance indicator has weak and insignificant correlations with the share of older adults, the share of children, and average years of schooling. In the post-disaster stage, disturbance intensity has significant negative correlations with the share of older adults and average years of schooling, and a weak negative correlation with the share of children. This indicates that during the disaster, travel disruption is less sensitive to demographic-structure bias and is driven mainly by sudden physical blockage; the invisibility of vulnerable groups in travel data has not yet been significantly amplified. In the post-disaster stage, correlations become stronger, suggesting that the method captures stronger socioeconomic sensitivity in the lagged recovery process and can partly identify differentiated effects of demographic structure on delayed disturbance. For example, streets with higher education levels, indicating fewer low-income residents, show higher post-disaster resilience.

However, the significant negative correlation with the share of older adults indicates a degree of representational bias in mobile phone signaling data at the neighborhood scale. Because older adults are underrepresented in the sample, travel reductions in some neighborhoods, such as Yuanling and Cuizhu subdistricts, contribute weakly to overall sample disturbance. This may produce a statistical illusion in which neighborhoods with more older adults appear more resilient. In other words, relying solely on mobile phone signaling data may underestimate the real disaster risks faced by vulnerable groups. Future studies should integrate community-level census or sample-survey data for calibration, so that resilience assessment becomes more inclusive.

Table 2. Correlation Analysis Between Average Street-Level Resilience and Demographic Structure Variables Across Different Stages

Demographic structure	Disaster-time per capita travel-	Post-disaster per capita travel-disruption

variable	disruption intensity	intensity
Share of population aged 65 and above	-0.152	-0.530*
Share of children aged 0-14	-0.007	-0.380
Average years of schooling among population aged 15 and above	-0.099	-0.582*

Note: * indicates significance at the 0.05 level (two-tailed).

4. Discussion and Conclusions

4.1 Main Conclusions and Practical Value

This study constructs a neighborhood pluvial flood resilience assessment framework based on the spatiotemporal disruption of residents' travel during rainstorm disasters and empirically tests it using Shenzhen's "9.7" extreme rainstorm. By analyzing mobile phone signaling data from approximately one million anonymized devices, the study constructs travel fluctuation curves before and after the disaster, quantifies resilience levels during and after the disaster, and generates neighborhood resilience maps. The validity of the method is tested using actual road-waterlogging data and demographic structure.

The results show that commodity-housing neighborhoods are more resilient than urban villages, and that commodity-housing neighborhoods built in different periods also show significant heterogeneity in resilience. Association analysis based on waterlogged roads confirms that road waterlogging is an important driver of residents' travel disruption during disasters and validates the effectiveness of the framework in identifying spatial differences in neighborhood resilience. At the same time, demographic validation using street-level population structure reveals that mobile phone signaling data may contain intrinsic bias when used for micro-scale resilience assessment, potentially underestimating the real risks of aging neighborhoods.

Most existing disaster-resilience assessments focus on macro-scale static evaluation. This study enables refined judgment at the neighborhood scale and highlights the advantages of dynamic and continuous time-series analysis based on residents' travel characteristics. Compared with existing big-data studies using resilience curves, the adaptive optimization proposed here provides a more insightful perspective for understanding the spatiotemporal heterogeneity of urban pluvial flood resilience and for supporting disaster emergency governance. Unlike elevation-dependent scenario simulation, this study not only verifies the significant association between disaster-time resilience and proximity to waterlogged roads, but also finds that low-resilience neighborhoods are not confined to a fixed distance from waterlogged roads (Figure 5). At the same time, although low-elevation neighborhoods are traditionally regarded as high-risk areas, the study finds that this assumption does not fully match actual resident travel disruption. Some neighborhoods near hillsides, for example, have relatively high terrain but low resilience because road choice is limited. Mobility-based dynamic assessment can therefore capture more complex impacts that traditional assessment may overlook.

This study also responds to the social-equity issue in urban resilience research. Existing research [15] indicates that socioeconomically disadvantaged neighborhoods often have lower resilience. By comparing neighborhoods of different construction periods and property types, this study further confirms the relationship between socioeconomic factors and resilience. It reflects the real differences in neighborhood resilience caused by infrastructure deficits and unequal resource allocation during disaster resistance and recovery. The neighborhood-level resilience maps also provide a more refined representation of resilience at the urban micro scale.

4.2 Suggestions for Incorporating Resilience Assessment into Neighborhood-Scale Urban Physical Examination

According to policy documents such as the Technical Guidelines for Urban Physical Examination and Evaluation in Territorial Spatial Planning, urban physical examination has become an important institutional tool for promoting high-quality urban development and addressing weaknesses in human settlements. Resilience is an important dimension of current urban physical examination. In response to the lack of systematic methods for fine-scale dynamic resilience assessment at the neighborhood scale, this study proposes a mobile-phone-signaling-data-driven procedure for neighborhood pluvial flood resilience examination and assessment. It can be piloted and promoted within urban physical examination.

For urban renewal and neighborhood disaster emergency management, the procedure includes data collection, baseline construction, disaster-stage division, disturbance quantification, and external validation. Diagnostic results can be fed back into urban physical examination information platforms and further embedded in the preparation of urban renewal plans. For example, low-resilience neighborhoods can be incorporated into urban renewal project databases and matched with progressive micro-renewal, blue-green infrastructure gap-filling, and community emergency coordination mechanisms. This can form a closed-loop governance pathway of "physical examination and assessment - diagnostic identification - prioritized and targeted rectification - dynamic monitoring," supporting data-driven routine monitoring, early warning, and sustainable planning decisions.

4.3 Research Limitations and Future Prospects

A decline in resident travel volume does not solely reflect impairment of neighborhood system functions. The travel-disruption intensity indicator used in this study does not distinguish between blocked compulsory travel and voluntary avoidance of flexible travel, which may underestimate the resilience of neighborhoods with strong governance capacity. Future research can develop multi-source data-fusion platforms integrating points of interest, land use, satellite remote sensing, mobile phone signaling, and social media data. LSTM time-series prediction or graph neural networks can be used to cluster travel trajectories and separately quantify compulsory and flexible mobility fluctuations, thereby providing more targeted decision support for resilience governance.

The core indicator V1 is useful for revealing the cumulative bearing capacity of neighborhoods under rainstorm disturbance, but a single indicator cannot fully balance acute risk and long-term cumulative loss. Future studies can construct composite indicators incorporating peak loss rate to capture maximum disaster intensity and acute risk, and combine recovery slope and curve-shape clustering to improve assessment accuracy while distinguishing mechanisms of acute-risk resistance and long-term recovery capacity across neighborhoods.

Notes

[1] Most waterlogging points were cleared within 48 hours, and emergency response intensity declined significantly. Water supply, power supply, communications, and other critical infrastructure returned

fully to normal within 72 hours. Source: Shenzhen Meteorological Bureau (Observatory), "Acting with the Wind, Fighting Wind and Rain, and Building the First Line of Urban Disaster Prevention and Reduction: A Record of the Shenzhen Meteorological Bureau's Response to Typhoon Saola and the '9.7' Extreme Heavy Rainstorm."

References

[1] CHEN Yi, CHEN Ruishan, GE Yi. Research and reflections on social vulnerability and resilience to flood disasters in China's urban communities[J]. Urbanism and Architecture, 2018(35): 32-34.

[2] CHEN Xunlai, XU Ting, WANG Rui, et al. Fine-scale observational characteristics and causes of the "9.7" extreme rainstorm in the Pearl River Delta[J]. Journal of Applied Meteorological Science, 2024, 35(1): 1-16.

[3] WEI Zongcai, LIN Yudong, WEN Xiaolan, et al. Research progress on urban resilience under extreme climate in China and abroad: conceptual frameworks, measurement, and optimization strategies[J]. Planners, 2025, 41(7): 10-17.

[4] CUTTER S L, FINCH C. Temporal and spatial changes in social vulnerability to natural hazards[J]. Proceedings of the National Academy of Sciences, 2008, 105(7): 2301-2306.

[5] BALICA S F, WRIGHT N G, VAN DER MEULEN F. A flood vulnerability index for coastal cities and its use in assessing climate change impacts[J]. Natural Hazards, 2012, 64: 73-105.

[6] ZHANG Xiaorui, ZHANG Linya, FANG Chuanglin. Concept, framework, and measurement: a review and extension of urban vulnerability research[J]. Geography and Geo-Information Science, 2015, 31(4): 94-99.

[7] CUTTER S L, BORUFF B J, SHIRLEY W L. Social vulnerability to environmental hazards[J]. Social Science Quarterly, 2003, 84(2): 242-261.

[8] CUTTER S L, BURTON C G, EMRICH C T. Disaster resilience indicators for benchmarking baseline conditions[J]. Journal of Homeland Security and Emergency Management, 2010, 7(1): 51.

[9] CUTTER S L, ASH K D, EMRICH C T. The geographies of community disaster resilience[J]. Global Environmental Change, 2014, 29: 65-77.

[10] TIMMERMAN P. Vulnerability, resilience and the collapse of society: a review of model's possible climatic applications[R]. Toronto: Institute for Environmental Studies, University of Toronto, 1981.

[11] ZHAI Guofang. Resilient responses to urban pluvial flood disasters from a planning perspective under climate change: key concepts, basic ideas, and a general framework[J]. Urban Planning Forum, 2024(1): 29-37.

[12] HOLLING C S. Resilience and stability of ecological systems[J]. Annual Review of Ecology and Systematics, 1973, 4: 1-23.

[13] ADGER W N. Social and ecological resilience: are they related?[J]. Progress in Human Geography, 2000, 24(3): 347-364.

[14] FOLKE C, CARPENTER S, WALKER B, et al. Regime shifts, resilience, and biodiversity in ecosystem management[J]. Annual Review of Ecology, Evolution, and Systematics, 2004, 35(1): 557-581.

[15] SHARIFI A, YAMAGATA Y. Urban resilience assessment: multiple dimensions, criteria, and indicators[M]//YAMAGATA Y, SHARIFI A. Urban resilience: a transformative approach. Cham: Springer, 2016.

[16] MEEROW S, NEWELL J P, STULTS M. Defining urban resilience: a review[J]. Landscape and Urban Planning, 2016, 147: 38-49.

[17] SPAANS M, WATERHOUT B. Building up resilience in cities worldwide: Rotterdam as participant in the 100 Resilient Cities Programme[J]. Cities, 2017, 61: 109-116.
[18] GUO Renzhong, YANG Xiaochun, HONG Wuyang, et al. Basic logic and framework for safe and resilient city planning and design[J]. Strategic Study of CAE, 2025, 27(4): 28-42.
[19] CHEN Bilin, LI Yinglong. Assessment of adaptive transformation planning for high-density coastal cities oriented toward flood resilience: a case study of Shenzhen Bay Mangrove Area[J]. Urban Planning Forum, 2023(4): 77-86.
[20] LIU C, XU F, GAO C, et al. Deep learning resilience inference for complex networked systems[J]. Nature Communications, 2024, 15(1): 9203.
[21] FAN Yating, LI Yuefan, TU Wei, et al. Vulnerability assessment of urban disaster-bearing bodies supported by social media data: a case study of extreme weather in Shenzhen[J]. City Planning Review, 2024, 48(08): 101-113.
[22] HSU C W, MOSTAFAVI A. Dissecting resilience curve archetypes and properties in human systems facing weather hazards[J]. Scientific Reports, 2025, 15(1): 11897.
[23] ZHANG F, LI Z, LI N, et al. Assessment of urban human mobility perturbation under extreme weather events: a case study in Nanjing, China[J]. Sustainable Cities and Society, 2019, 50: 101671.
[24] TANG J, ZHAO P, GONG Z, et al. Resilience patterns of human mobility in response to extreme urban floods[J]. National Science Review, 2023, 10(8): nwad097.
[25] BRUNEAU M, CHANG S E, EGUCHI R T, et al. A framework to quantitatively assess and enhance the seismic resilience of communities[J]. Earthquake Spectra, 2003, 19(4): 733-752.
[26] HONG B, BONCZAK B J, GUPTA A, et al. Measuring inequality in community resilience to natural disasters using large-scale mobility data[J]. Nature Communications, 2021, 12(1): 1870.
[27] OUYANG M, DUEÑAS-OSORIO L, MIN X. A three-stage resilience analysis framework for urban infrastructure systems[J]. Structural Safety, 2012, 36: 23-31.
[28] REED D A, KAPUR K C, CHRISTIE R D. Methodology for assessing the resilience of networked infrastructure[J]. IEEE Systems Journal, 2009, 3(2): 174-180.
[29] QIAN J, DU Y, LIANG F, et al. Measuring community resilience inequality to inland flooding using location aware big data[J]. Cities, 2024, 149: 104915.
[30] YAN Wentao, REN Jie, ZHANG Shangwu, et al. Shanghai resilient city planning: key issues, overall framework, and planning strategies[J]. Urban Planning Forum, 2022(3): 19-28.
[31] YANG Junyan, CAO Jun. Dynamic, static, explicit, and implicit: four application modes of big data in urban design[J]. Urban Planning Forum, 2017(4): 39-46.
[32] PENG Chong, ZUO Peiwen, LI Yuewen, et al. Multi-risk coupling in urban space and resilient planning responses[J]. Urban Planning Forum, 2024(5): 88-97.
[33] PAN Haixiao, DAI Shenzhi, ZHAO Yanjing, et al. Academic discussion on "urban resilience and spatial planning in response to climate change"[J]. Urban Planning Forum, 2021(5): 1-10.
[34] NAN C, SANSAVINI G. A quantitative method for assessing resilience of interdependent infrastructures[J]. Reliability Engineering & System Safety, 2017, 157: 35-53.
[35] POULIN C, KANE M B. Infrastructure resilience curves: performance measures and summary metrics[J]. Reliability Engineering & System Safety, 2021, 216: 107926.
AI-assisted translation